RGNZ/MGPB

Geomechanical Analysis to Determine The Maximum Limit of Water Injection in the Keutapangan Formation, "ZA" Field, North Sumatra Basin

Rudarsko-geološko-naftni zbornik
(The Mining-Geology-Petroleum Engineering Bulletin)
DOI: 10.17794/rgn.2026.2.1

Original scientific paper

Zahra Adinda Billqish[1], Andika Wicaksono[2], Sismanto Sismanto[1]*

[1] *Geophysics Laboratory, Department of Physics, Faculty of Mathematics and Natural Sciences, Universitas Gadjah Mada, Jl. Geografi, Yogyakarta, 55281, Indonesia.*

[2] *Pertamina Hulu Rokan, Jl. Prof. DR. Satrio no. 30, Jakarta, Indonesia.*

Abstract

The "ZA" Field is located in the North Sumatra Basin and is predominantly affected by geopressure issues. As such, geomechanical analysis is crucial during drilling operations to mitigate potential hazards. The geomechanical analysis conducted in this study utilizes a 1D Mechanical Earth Model (MEM), which includes the following components: overburden stress, pore pressure, rock strength, rock elastic properties, and minimum horizontal stress. The data used in this analysis were obtained from the following sources: wireline logging for all geomechanical calculations, pressure tests to validate pore pressure values, fracture gradient data to validate the minimum horizontal stress curve, step-rate tests to determine the injection pressure limit, and well reports. The "ZA" Field exhibits a complex geopressure regime, ranging from underpressure to overpressure, with transitional zones that combine both conditions. Overpressure is primarily attributed to loading mechanisms, while underpressure results from historical fluid extraction during previous drilling activities. Lithological analysis indicates that the reservoir consists of shaly sand and fine-grained formations. Due to the shallow burial depth, these rocks remain poorly consolidated, resulting in a narrow safe injection window above the pore pressure. This constraint is exemplified by one well, where the maximum allowable injection pressure was 7.63 MPa, with only a 2 MPa margin above the pore pressure.

Keywords:
1D MEM, pore pressure, rock strengths, rock elastic properties, minimum horizontal stress

1. Introduction

Geomechanics plays a crucial role in minimizing hazards during drilling operations. It is used to analyze fault seal potential, predict pore pressure, assess wellbore stability, and evaluate various stimulation methods (**Lanin, 2021**). With current technological advancements, various methods have been applied in geomechanical data processing, one of which is machine learning-based approaches such as real-time LWD analysis. This technology enables the rapid and accurate estimation of geomechanical parameters, thereby supporting more effective, safe, and efficient decision-making during drilling operations and reservoir management (**Liu et al., 2025**). Neglecting geomechanical considerations has led to numerous incidents, including the Lapindo mudflow disaster. This disaster was triggered by subsurface overpressure, where the drilling mud weight was insufficient to counteract the formation pressure. As a result, the high-pressure mud erupted to the surface (**Nuraini, 2023**). This incident underscores the importance of geomechanical applications, particularly developing a Mechanical Earth Model (MEM), to mitigate subsurface risks.

The Mechanical Earth Model (MEM) is a comprehensive representation of rock mechanical properties, fracture behaviour, and subsurface stresses, pressures, and temperatures at depth. Geoscientists use MEM to predict rock deformation and failure during drilling. MEM integrates geological, geophysical, and field measurement data, including core tests, well logs, drilling records, and production data (**Zain et al., 2020**). Additionally, MEM helps estimate the maximum allowable fluid injection pressure, which must be carefully calibrated based on reservoir pore pressure and in-situ stress conditions. Excessive injection pressure can fracture cap rocks, leading to fluid leakage into unintended formations (**Rozamuri et al., 2022**). Mechanical Earth Models (MEMs) can be categorized into one-dimensional (1D) and three-dimensional (3D) models. The 1D MEMs demonstrate significant potential in addressing various challenges associated with reservoir planning and management. Furthermore, they also serve as a foundational step toward the development of 3D MEMs. This pro-

* Corresponding author: Sismanto
e-mail address: sismanto@ugm.ac.id
Received: 5 May 2025. Accepted: 20 September 2025.
Available online: 13 March 2026

gression can enhance the understanding of reservoir behaviour and improve predictive capabilities in geologically complex environments (**Verma et al., 2021**).

Previous geomechanical studies on the Keutapang Formation were conducted by **Aziz & Bolt (1984)** and **Yosandian et al. (2014)**. **Aziz & Bolt (1984)** attributed overpressure in the formation to high sedimentation rates and recommended a mud weight of 16.5 ppg for safe drilling. Similarly, **Yosandian et al. (2014)** confirmed overpressure in the Keutapang Formation, with density-sonic transit time cross-plots showing no evidence of mineral transformation. Another geomechanical study was conducted in southwest Iran, which used 1D MEMs to predict pressure and deformation changes, also assess the risk of fault reactivation and caprock stability. This approach can recognize the risk management of injection in old reservoirs. Although the processing is easier, if the data is incomplete, it can make the model less accurate and the risk of failure increases due to extreme conditions that cannot always be predicted (**Saadatnia et al., 2023**). This study aims to further investigate subsurface conditions through geomechanical analysis and determine the maximum safe injection pressure limit Keutapangan Formation, "ZA" Field, North Sumatra Basin.

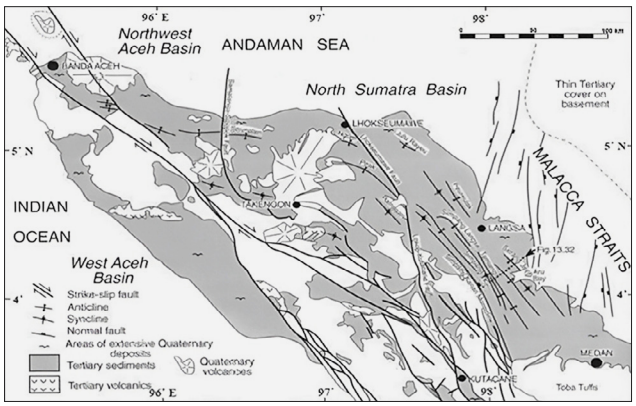

Figure 1. North Sumatra Basin (**Wardhana et al., 2021**)

2. Geological Setting

The North Sumatra Basin is one of Sumatra's three back-arc basins, situated along the western margin of Sundaland and spanning approximately 60,000 km², covering both onshore and offshore areas (**Tampubolon et al., 2017**). It is bounded by (see **Figure 1**); The Barisan Mountains to the southwest (SW), the Asahan Arch to the southeast (SE), the Andaman Sea to the northwest (NW), and the Malacca Platform to the northeast (NE).

The basin's dominant structural trends align in NW-SE and NE-SW directions. As shown in **Figure 1**, the North Sumatra Basin lies within a tectonically active zone on the western edge of the Sibumasu Block, where multiple tectonic events have significantly influenced its geological evolution. The basin's complex structural framework results from rotational and translational movements of major tectonic plates (**Wardhana et al., 2021**). The basin's tectonic model is primarily governed

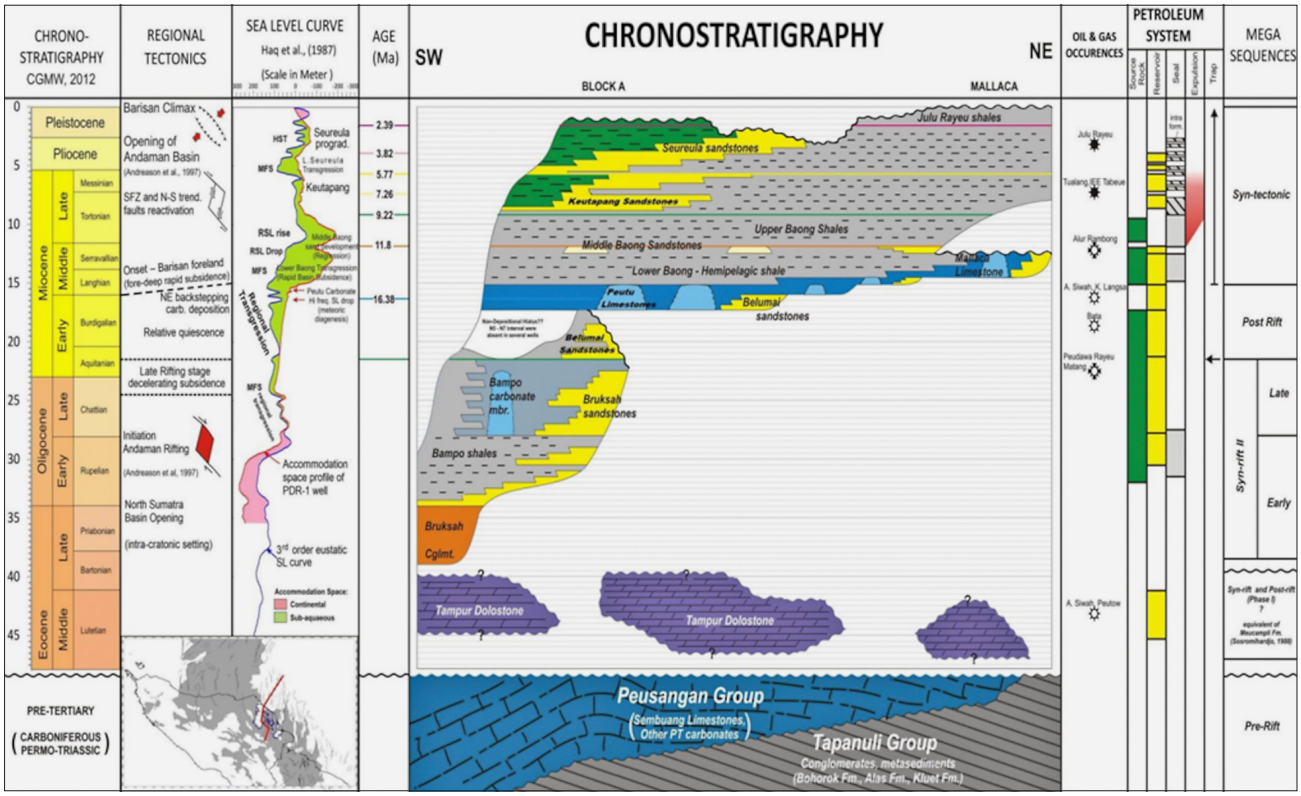

Figure 2. Basin stratigraphy (**Syarifuddin et al., 2018**)

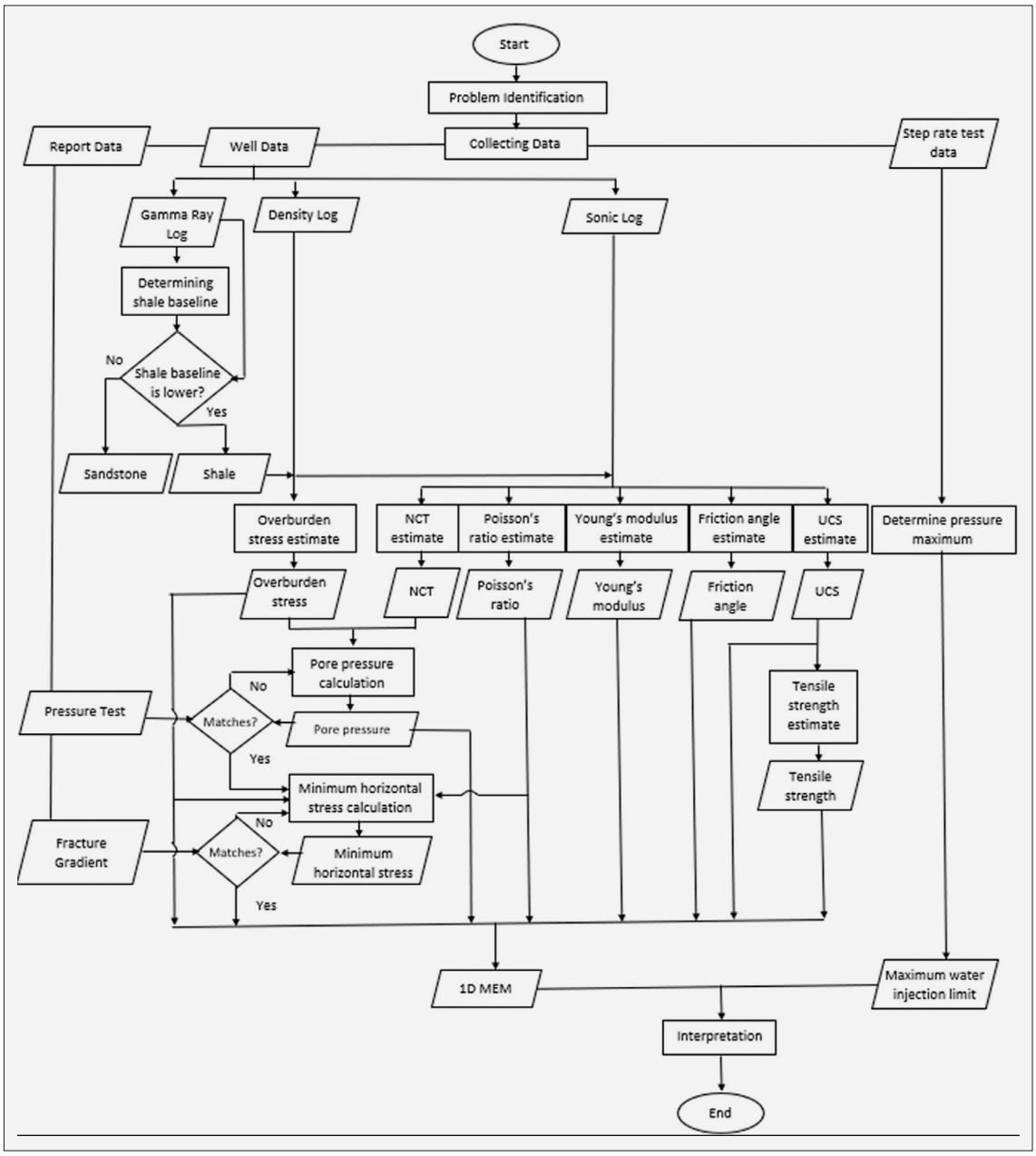

Figure 3. Flowchart

by a dextral strike-slip fault system (**Wardhana et al., 2021**).

Based on the stratigraphic column of the North Sumatra Basin (see **Figure 2**), nine formations have been identified:

1. Tampur-Meucampli Formation: composed of carbonate and dolomite sediments with chert nodules, deposited in sublittoral to marine environments. It is located on the eastern high of the basin near the Asahan Arch.
2. Meucampli Formation: consists of clastic sediments exposed in northwest Aceh
3. Parapat/Bruksah Formation: dominated by conglomerates and sandstones, with sandstone derived from local horst block contributions.
4. Bampo Formation: characterized by poorly laminated, pyritic carbonate shale with low carbonate content (**Muchlis & Elder, 2020**)
5. Peutu-Belumai Formation: consists of claystone and siltstone, moderately to highly calcareous, often fossil-rich, and slightly glauconitic (**Soepardji, 1983**). Belumai Formation: Comprises fine-to medium-grained sandstones, located in the eastern shelf area of the basin
6. Baong Formation: composed of shale, sandstone, and mudstone (**Wardhana et al., 2021**).
7. Keutapang Formation: features fine sandstone and clay with interbedded shale and thin limestone layers (**Prasetyo et al., 2021**).

8. Seurula Formation: consists of sandstone, shale, and clay
9. Julu Rayeu Formation: comprised of fine- to coarse-grained sandstone and claystone (**Astawa et al., 2012**).

3. Materials and Methods

This research involves 26 wells across the North Sumatra Basin. The data used includes wireline logging, pressure test, fracturing report, and well reports. The wireline logging data used comprises gamma ray logs, sonic logs, and density logs, all of which are available for every well. Pressure test data only available for one well (Well-23) and fracturing report data, includes step rate test data and fracture gradient, is available for only one well (Well-7). All geomechanical data calculations were performed in Microsoft Excel, where the processing flow can be seen in **Figure 3**.

The data limitations and applications are that the limited availability of pressure test data (only one well) limits its direct comparisons across the field and prevents extrapolation to other wells, single-well step rate test is applied conservatively and locally without generalization to field-wide operations, and fracture gradient data serves as key validation for stress field modelling. The integration of these datasets enables robust pore pressure prediction through Eaton's method with empirical validation, accurate determination of injection pressure limits for reservoir management, and comprehensive stress field characterization for wellbore stability analysis

All data processing and interpretations follow standard petroleum engineering protocols, with quality control measures applied to ensure data reliability. Where data is limited (pressure tests, step rate tests), conservative engineering approaches are employed to mitigate uncertainty. While this study does not include direct validation using numerical simulations, core-based MEMs, or machine learning approaches, the mechanical parameters and equations adopted in the 1D MEM construction are consistent with widely accepted geomechanical modelling practices as demonstrated in numerous previous studies, such as **Zain et al. (2020)**, **Shen et al. (2024)**, and **Larsen et al. (2000)**.

Overburden stress is caused by the weight of the overlying formation layers. Density logs are typically used to determine the overburden stress. The value of the overburden stress can be obtained using the equation (**Knoll, 2016**),

$$\sigma_v = \int_0^z \rho(z) g dz \quad (1)$$

Where:

σ_v – overburden stress (Pa),
$\rho(z)$ – bulk density (kg/m^3),
z – depth (m),
g – gravity constant (m/s^2).

Hydrostatic pressure is caused by static or non-moving fluid at a certain depth (**Wicaksono, 2021**). Hydrostatic pressure is defined by

$$P = \rho_w g z \quad (2)$$

Where:

P – hydrostatic pressure (Pa),
ρ_w – water density (kg/m^3),
g – gravity constant (m/s^2),
z – depth (m).

The Normal Compaction Trend (NCT) represents a linear relationship derived from optimally compacted intervals in low-permeability formations. This fundamental geomechanical parameter serves two critical functions, i.e. baseline reference for normal pressure conditions, and a diagnostic tool for identifying geopressure zones where pore pressure exceeds hydrostatic pressure (see **Figure 4**).

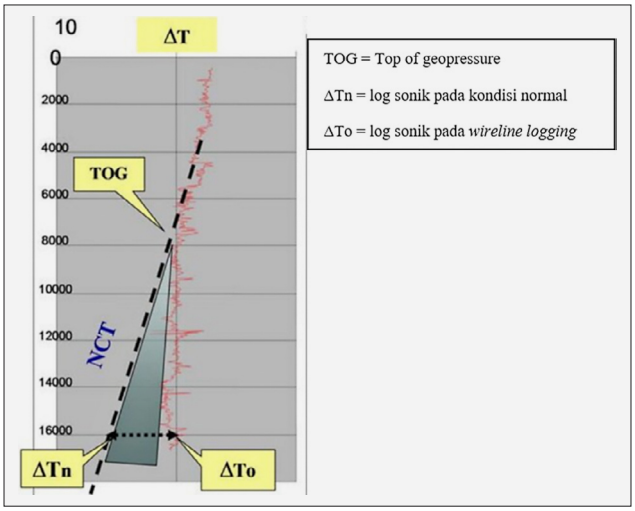

Figure 4. Pore pressure prediction based on NCT (**Shaker, 2007**)

Key characteristics of NCT exhibit an exponential decrease with depth, it requires Δt_mudline (sonic transit time at mud-line) as the input parameter, typical range of 185-200 μs/ft (**Zhang, 2013**), and formation-specific variations may occur based on lithology.

In pore pressure prediction, the primary reference for Eaton's method calculations and critical for identifying transition zones between pressure regimes, enables the detection of under-compaction anomalies (**Shaker, 2007**). The NCT curve's reliability depends on the quality of sonic log data, proper selection of reference shales, and accounting for regional geological variations. This methodology provides the foundation for accurate pore pressure prediction, essential for well planning and drilling hazard mitigation.

$$\Delta t_n = \Delta t_m + (\Delta t_{ml} - \Delta t_m) e^{-cz} \quad (3)$$

Where:

Δt_n – transit time value in Normal Compaction Trend (μs/ft),

Δt_m – transit time value in wireline logging (μs/ft),
Δt_{ml} – transit time value of mudline (μs/ft),
c – constant,
z – depth (m).

Pore pressure refers to the fluid pressure within rock pore spaces. Under normal hydrostatic conditions, it equals the pressure exerted by a vertical column of formation water. Direct measurement techniques include Repeat Formation Tester (RFT), and Modular Dynamic Tester (MDT**) (Wicaksono, 2021**). Wireline log-based pore pressure calculations achieve greater accuracy in shale intervals than in sandstone due to fundamental differences in compaction behaviour:

Especially in Shale Characteristics: extremely low permeability inhibits fluid escape, mechanical compaction under overburden stress leads to fluid retention and pressure buildup, and diagenetic processes can further enhance overpressure conditions. While for Sandstone behaviour, higher permeability enables fluid redistribution, and rapid pressure equalization occurs despite diagenetic effects (**Osborne, 1997**).

The Eaton method was developed for the Gulf of Mexico's undercompacted, overpressured shales. This widely used technique derives from the principle of effective stress. The method can be identified the specifically designed for shale formations; incorporates sonic, resistivity, or density log data; relies on normal compaction trend analysis; and is particularly effective in young, Tertiary basins.

This equation to approach remains fundamental in modern pore pressure prediction workflows, though it requires careful calibration with direct pressure measurements in each basin.

$$\sigma_{eff} = \sigma_v - P_p \tag{4}$$

Where:

σ_{eff} – effective stress (Pa),
σ_v – overburden stress (Pa),
P_p – pore pressure (Pa).

Terzaghi's principle states that when a rock experiences vertical stress, that stress is countered by the pore fluid pressure within the rock, which consists of pore pressure and effective stress. Effective stress can be correlated with log data such as resistivity, wave velocity, or transit time to establish the Eaton relationship in (**Knoll, 2016**)

$$P_p = \sigma_v - (\sigma_v - P)\left(\frac{\Delta t_m}{\Delta t_n}\right)^n \tag{5}$$

Where:

σ_v – overburden stress (Pa),
P – hydrostatic pressure,
Δt_m – transit time value in wireline logging (μs/ft),
Δt_n – transit time value in Normal Compaction Trend (μs/ft),
n – constant that is used for calibration.

The elastic properties of rocks can be classified into static and dynamic elastic properties. Static elastic properties are obtained through core analysis to determine Young's modulus and Poisson's ratio, with depth-specific information limited to the locations where core samples are taken. In contrast, dynamic elastic properties are derived from sonic log measurements (**Knoll, 2016**). Based on laboratory testing, static and dynamic elastic properties are not identical due to differences in strain magnitude. The measured modulus is not purely elastic, as it includes additional irreversible deformation caused by friction. This indicates that static strain is always greater than dynamic strain, resulting in static elastic modulus values that are consistently lower than dynamic elastic modulus values (**Knoll, 2016**). The equation for static Young's modulus is presented in (**Amin et al, 2022**);

$$E_s = \left(0.076 \times \left(\frac{304.8}{\Delta t_p}\right)^{3.23}\right) \tag{6}$$

Where:

E_s – static young modulus (GPa),
Δt_p – slowness of compression wave (μs/ft).

Poisson's ratio is defined as the (negative) ratio of lateral strain to axial strain under uniaxial stress conditions (**Tandirerung, 2023**). The equation for Poisson's ratio is presented in **Christaras et al. (1994)**;

$$\nu_{sta} = 0.71\nu_{dyn} + 0.063 \tag{7}$$

Where:

ν_{sta} – static Poisson ratio and ν_{dyn} – dynamic Poisson ratio.

Rock strength is the ability of a rock to resist external deformation when subjected to external stress (**Gunawan et al., 2017**). Rock strength can be represented by unconfined compressive strength (UCS), tensile strength, and friction angle. An empirical approach is commonly applied using various correlation methods. One such technique involves relating uniaxial compressive strength (UCS) to the compressional wave transit time interval, as shown in Equation 8 (**Amin et al., 2022**). Rock strength based on UCS is classified into four categories, as presented in **Table 1** (**Attewell & Farmer, 1976**).

Rock strength refers to a formation's capacity to withstand external stresses without permanent deformation (**Gunawan et al., 2017**). This fundamental geomechanical property is typically quantified through three key parameters;

1. Strength Parameters (Unconfined Compressive Strength (UCS), Tensile Strength, and Internal Friction Angle).
2. Empirical Determination Methods (The most common approach utilizes established correlations, including UCS derivation from compressional wave (P-wave) transit time (Δt) (**Amin et al., 2022**), and other log-derived relationships (sonic, density, or resistivity-based).

Table 1: Rock strength classification based on UCS (**Attewell & Farmer, 1976**)

Strength Classification	Strength Range (MPa)	Typical Rock Types
Very weak	10-20	Weathered and weakly compacted sedimentary rocks
Weak	20-40	Weakly-cemented sedimentary rocks, schist
Medium	40-80	Competent sedimentary rocks, some low-density coarse-grained igneous rocks
Strong	80-160	Competent igneous rocks, some metamorphic rocks, and fine-grained sandstones

3. UCS Classification System: Attewell and Farmer's (1976) classification, as referenced in **Wilson et al. (2022)**, categorizes rock strength into four distinct classes based on UCS magnitude (see **Table 1**)

This classification system provides essential guidance for Wellbore stability analysis, Hydraulic fracturing design, Sand production prediction, and Drilling parameter optimization

The empirical correlations remain particularly valuable when core data is unavailable, though they require regional calibration for optimal accuracy in different geological settings (**Moos et al., 1999** in **Knoll. 2016**).

$$UCS = 42.1 \exp\left(1.9 \times 10^{-11} \rho {V_p}^2\right) \quad (8)$$

Where:

UCS – unconfined compressive strength (MPa),

ρ – density log (g/cm^3),

V_p – compressional wave velocity (m/s).

Tensile strength is defined as the maximum amount of tensile stress that a material can withstand before failure occurs. In the context of rock mechanics, tensile strength is crucial as it affects the stability and integrity of rock structures (**Perras & Diederichs, 2014**). According to **Perras & Diederichs (2014)**, an empirical equation for tensile strength is presented in;

$$T = \frac{1}{10} \times UCS \quad (9)$$

Where:

T – tensile strength (MPa),

UCS – unconfined compressive strength (MPa).

The tensile strength can be classified for various rock types based on **Lockner (1995)**, as shown in **Figure 5**.

The friction angle is a measure of a rock's ability to resist shear stress. It represents the ratio between the normal force and the resultant force during failure caused by shear stress. The friction angle, along with UCS, is essential for many commonly used failure criteria to estimate rock strength at depth. An empirical equation to calculate the friction angle is presented in **Zain et al. (2020)**;

$$\varphi = 26.5 - 37.4\left(1 - \phi - V_{clay}\right) + \\ + 62.1\left(1 - \phi - V_{clay}\right)^2 \quad (10)$$

Where:

φ – friction angle (°),

ϕ – porosity,

V_{clay} – volume of clay.

Based on **Linh et al. (2021)**, the friction angle is categorized into three groups, as shown in **Table 2.**

Minimum horizontal stress represents the threshold at which rock begins to fracture, indicating the rock's strength limit (**Wicaksono, 2021**). This stress can be measured using extended leak-off tests (XLOT) or mini-frac tests. In these methods, fluid is injected into the wellbore to pressurize the exposed rock interval until fracturing occurs. As pumping continues at a constant rate, the fracture propagates away from the wellbore.

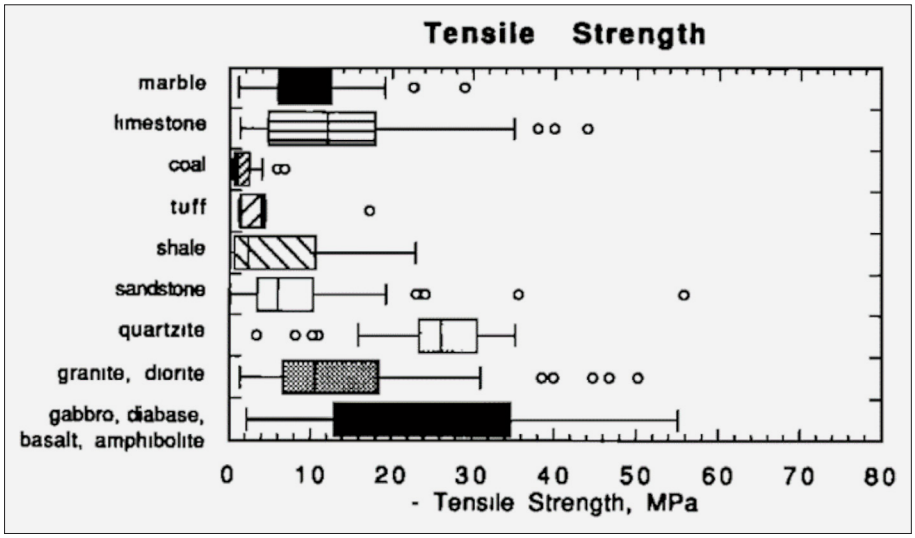

Figure 5. Classification of tensile strength (**Lockner, 1995**)

Table 2. Classification of friction angle (**Linh et al., 2021**)

Classification	Friction angle (degree)	Type of rock
Low	20-27	Schist (mica), clay, marl
Medium	27-34	Sandstone, siltstone, chalk, gneiss, slate
High	34-40	Basalt, granite, limestone, and conglomerate

The fracture grows in a direction perpendicular to the least principal stress, as this orientation requires the least energy for propagation. Consequently, the pressure required to propagate the fracture is equal to or greater than the minimum horizontal stress (**Knoll, 2016**).

Fracture propagation will cease when the rate of fluid leakage from the fracture and wellbore into the formation exceeds the rate of fluid injection. If pumping is stopped, fluid continues to leak from the fracture walls until the fracture closes and becomes disconnected from the wellbore. The fracture closes once the pressure falls below the normal stress acting on it, which corresponds to the minimum horizontal stress, and the value of the minimum horizontal stress can be calculated using an equation (**Knoll, 2016**),

$$S_{hmin} = \frac{\nu}{1-\nu}\left(\sigma_v - P_p\right) + P_p \tag{11}$$

Where:

S_{hmin} – minimum horizontal stress (Pa),

ν – poisson ratio,

σ_v – overburden stress (Pa),

P_p – pore pressure (Pa).

The injection pressure window refers to the pressure range used to inject fluid into the reservoir, where the pressure must be high enough to induce shear failure and enhance permeability, yet low enough to avoid damaging the formation. Elevated injection pressures can trigger shear failure, thereby improving permeability. An effective degree of shear failure can be achieved by maintaining injection pressures within this optimal window (**Collins, 2002**).

Determining the appropriate injection pressure window requires an understanding of both the pore pressure and the minimum horizontal stress. Pore pressure represents the fluid pressure within the formation, while the minimum horizontal stress defines the lower bound beyond which rock fracturing will occur.

Underpressure is defined as a pressure that is lower than hydrostatic pressure. It typically occurs when fluids are extracted from a reservoir, leading to a reduction in fluid volume and, consequently, a decrease in pore pressure. This phenomenon is commonly observed in depleted fields – reservoirs that have already produced oil and gas.

In addition to production-related causes, underpressure can also occur naturally. Naturally occurring underpressure can be classified into gravity-driven and geologically driven processes. Gravity-driven underpressure arises from changes in elevation, flow rates, or the selected reference for the hydrostatic gradient. In contrast, geologically induced underpressure results from geological changes that alter the intrinsic properties of rocks or the pressure–volume–temperature (PVT) conditions of fluids, preventing the fluid pressure from equilibrating with its surroundings (**Birchall et al., 2022**).

Overpressure can be categorized into two main mechanisms: loading and unloading. The loading mechanism (see **Figure 6a**) is typically caused by rapid sedimentation in a basin, during which the fluids within the rock pores are unable to escape – a process known as disequilibrium compaction. This mechanism generally produces consistent patterns in sonic and density logs, reflecting the imbalance between fluid retention and the rate of pore compaction. As sediment accumulates, vertical stress – or gravitational loading – increases, potentially generating excess pressure due to uneven compaction (**Buntoro et al., 2022**).

The unloading mechanism (see **Figure 6b**), on the other hand, contributes to overpressure through processes that transfer the load from grain-to-grain contact within the rock to the fluids occupying the pores (**Buntoro et al, 2022**). This can occur when pore fluids are introduced or when part of the solid matrix spontaneously transforms into fluid, increasing pore pressure – assuming the fluid cannot escape. In such cases, a portion of the stress previously supported by the rock

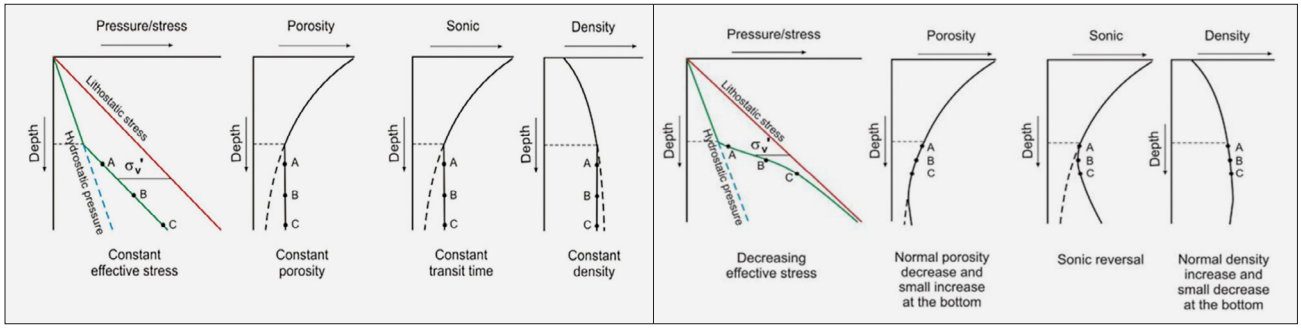

Figure 6. Overpressure mechanism a) Loading mechanism b) Unloading mechanism

framework is transferred to the pore fluid, resulting in elevated pore pressure due to load redistribution (**Buntoro et al., 2022**).

4. Results and Discussion

4.1. Analysis of 1D Mechanical Earth Model

This study presents a one-dimensional geomechanical model analysis conducted on 26 wells within the Keutapang Formation of the 'ZA' Field, located in the North Sumatra Basin. The analysis encompasses pore pressure, elastic properties, rock strength, the injection pressure window, and injection pressure limits.

The pore pressure anomalies identified in this study are classified into three categories: underpressure, overpressure, and a combination of overpressure and underpressure. Each well exhibits distinct pore pressure behaviour at various depths, as summarized in **Table 3**.

Table 3. Depth of overpressure-underpressure in each well

Wells	Pore Pressure Problem	Depth of Pore Pressure (m)
ZA-3	*Underpressure*	440-640
ZA-5	*Underpressure*	500-680
ZA-21	*Underpressure*	410-540
ZA-22	*Underpressure*	425-580
ZA-26	*Underpressure*	340-710
ZA-1	*Overpressure*	550-630
ZA-6	*Overpressure*	320-430
ZA-7	*Overpressure*	630-750
ZA-8	*Overpressure*	350-590
ZA-11	*Overpressure*	470-510
ZA-13	*Overpressure*	340-600
ZA-16	*Overpressure*	250-310 & 420-540
ZA-20	*Overpressure*	300-390
ZA-2	*Overpressure-Underpressure*	530-570 ; 590-830
ZA-4	*Overpressure-Underpressure*	490-560 ; 655-835
ZA-9	*Overpressure-Underpressure*	500-560 ; 660-750
ZA-10	*Overpressure-Underpressure*	520-570 ; 600-660
ZA-12	*Overpressure-Underpressure*	490-560 ; 560-720
ZA-14	*Overpressure-Underpressure*	490-540 ; 590-735
ZA-15	*Overpressure-Underpressure*	470-520 ; 590-750
ZA-17	*Overpressure-Underpressure*	480-530 ; 620-680
ZA-18	*Overpressure-Underpressure*	465-510 ; 560-710
ZA-19	*Overpressure-Underpressure*	470-520 ; 720-790
ZA-23	*Overpressure-Underpressure*	540-560 ; 590-710
ZA-24	*Overpressure-Underpressure*	550-595 ; 595-720
ZA-25	*Overpressure-Underpressure*	490-530 ; 560-730

Out of the 26 wells analyzed, three representative wells are selected to illustrate each type of pore pressure condition. **Figure 7** presents an example of a one-dimensional Mechanical Earth Model (MEM) curve displaying an underpressure condition. Underpressure occurs when the pore pressure is lower than the hydrostatic pressure. As shown in **Figure 7**, the pore pressure (green curve) lies to the left of the hydrostatic pressure (red curve).

The underpressure mechanism observed in the study area is attributed to fluid extraction from the reservoir during past production activities. This condition commonly arises in depleted fields, where reduced fluid volume within the rock leads to a drop in pore pressure. As the amount of fluid in the pore spaces becomes insufficient to support the overburden pressure, underpressure conditions are developed.

Figure 8 presents a sample of one-dimensional Mechanical Earth Model (MEM) curves illustrating an overpressure condition. Overpressure occurs when the pore pressure exceeds the hydrostatic pressure. As shown in **Figure 8**, the pore pressure (green curve) is positioned to the right of the hydrostatic pressure (red curve).

The overpressure mechanism observed in the study area is attributed to a sedimentation rate that outpaces the rate at which fluids can escape from the rock pores, a process referred to as the loading mechanism. This typically occurs at relatively shallow formation depths. In such cases, fluids become trapped within the rock matrix rather than being expelled, resulting in a buildup of pore pressure and the development of overpressure.

Figure 9 presents a sample of one-dimensional Mechanical Earth Model (MEM) curves illustrating a combined overpressure–underpressure condition. Overpressure occurs when the pore pressure exceeds the hydrostatic pressure, while underpressure occurs when the pore pressure falls below the hydrostatic pressure. As shown in **Figure 9**, the pore pressure (green curve) lies both to the right and left of the hydrostatic pressure (red curve). The overpressure observed in the study area is attributed to a sedimentation rate that exceeds the rate of fluid expulsion from the rock pores, a process commonly referred to as the loading mechanism. In contrast, the underpressure condition is linked to fluid extraction from the reservoir during past production activities. The presence of both overpressure and underpressure within a single well may result from rapid sedimentation overlying an underpressured formation.

4.2. Analysis of Rock Elastic Properties and Rock Strengths

The wells in this field exhibit a relatively consistent range of elastic properties and rock strength. Young's modulus values range from 0.5 to 2 GPa, while Poisson's ratio is approximately 0.2. These values suggest that the rocks are relatively deformable and susceptible to fracturing.

In terms of rock strength, the wells display unconfined compressive strength (UCS) values in 42 MPa,

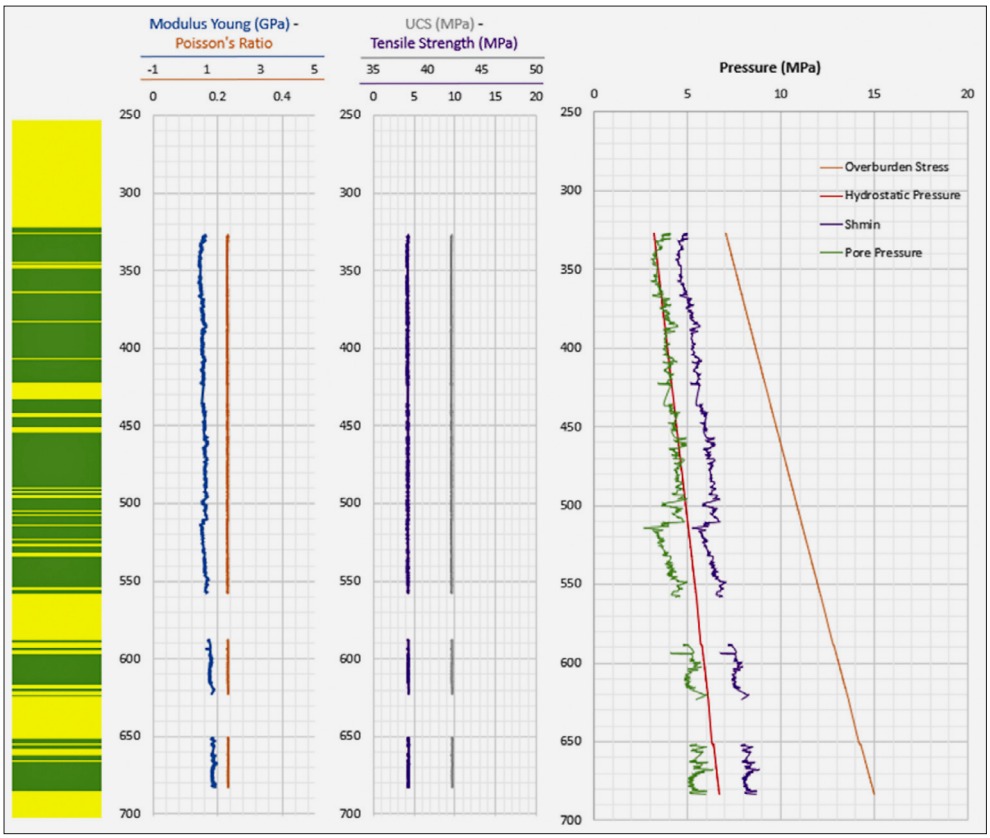

Figure 7. 1D MEM of ZA-5 well

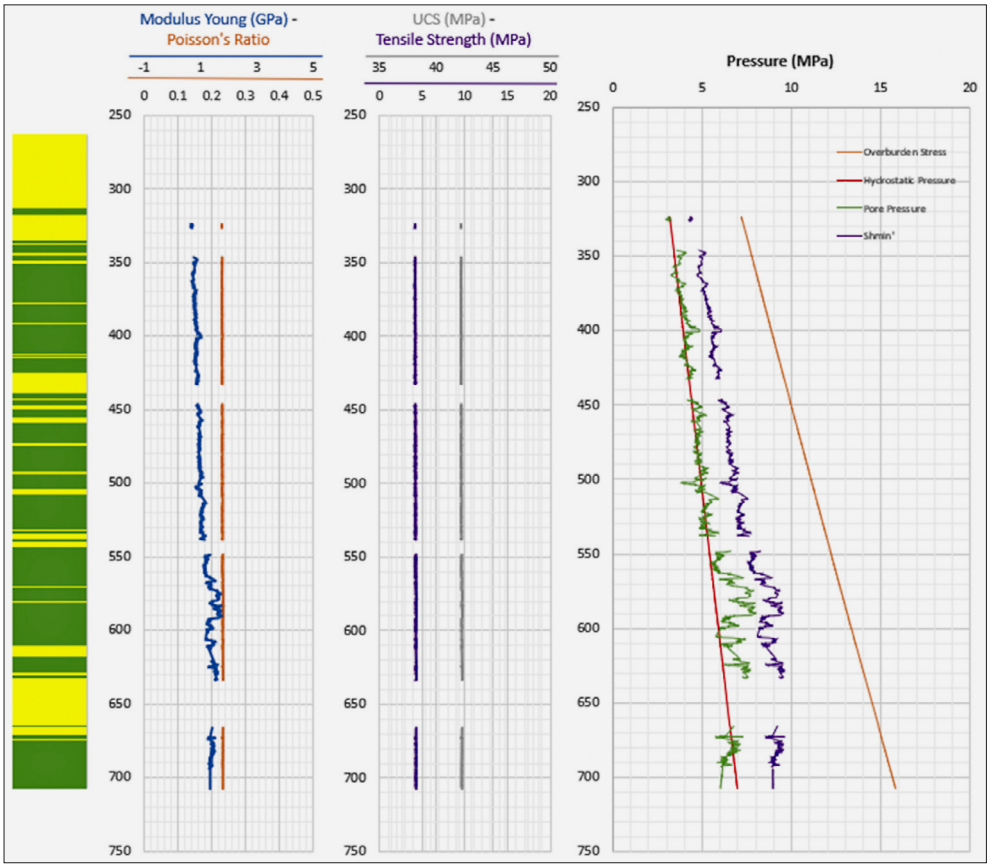

Figure 8. 1D MEM of ZA-1 well

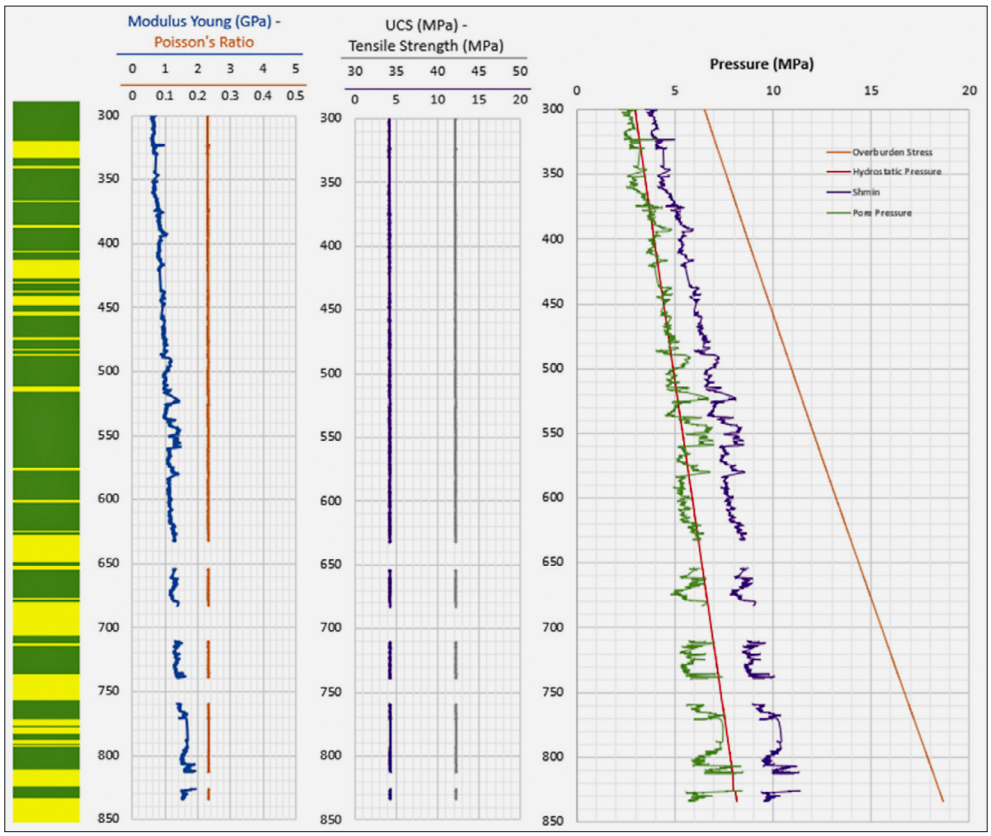

Figure 9. 1D MEM of ZA-4 well

Table 4. Rock strength for each well

Sumur	UCS (MPa)	*Tensile strength (MPa)*	*Friction angle (°)*
ZA-3	42	4	22-29
ZA-5	42	4	22-26
ZA-21	42	4	20-32
ZA-22	42	4	20-30
ZA-26	42	4	20-27
ZA-1	42	4	21-30
ZA-6	42	4	21-26
ZA-7	42	4	20-35
ZA-8	42	4	22-26
ZA-11	42	4	22-30
ZA-13	42	4	21-29
ZA-16	42	4	21-25
ZA-20	42	4	20-25
ZA-2	42	4	21-31
ZA-4	42	4	20-23
ZA-9	42	4	20-29
ZA-10	42	4	21-26
ZA-12	42	4	21-26
ZA-14	42	4	21-31
ZA-15	42	4	21-25
ZA-17	42	4	21-25
ZA-18	42	4	22-28
ZA-19	42	4	21-27
ZA-23	42	4	20-28
ZA-24	42	4	20-29
ZA-25	42	4	20-24

tensile strength in 4 MPa, and friction angles ranging from 20° to 31°. Detailed rock strength values for each well are provided in **Table 4**.

These data indicate that the formations are composed of weak sedimentary rocks with a shaly sand lithology. This lithology, characterized by fine grain size, tends to be more resistant to deformation if the rocks are well-compacted. However, in these wells, the rocks are not yet fully compacted, as evidenced by the relatively low friction angles. A low friction angle implies that the rock grains can be easily displaced under shear stress.

4.3. Analysis of Injection Window and Limit

The injection window is defined by the pressure range between the pore pressure (formation pressure) and the minimum horizontal stress, or fracture gradient. The minimum horizontal stress tends to approximate the overburden pressure at greater depths and the hydrostatic pressure at shallower depths. In this field, the injection window is relatively wide, encompassing both overpressure (1–2 MPa) and underpressure (1.5–5 MPa). The injection window for each well is detailed in **Table 5**.

Based on these values, the formations in this field are considered to be relatively shallow, as the pressures are closer to hydrostatic pressure than to overburden pressure. In addition to the injection window, this study also identifies the maximum injection limit. This limit is determined from the maximum pressure step-rate test, which is avail-

Table 5. Injection window for each well

Wells	Injection Window (MPa)	Pore Pressure	Depth of Pore Pressure (m)
ZA-3	2.5	underpressure	440-640
ZA-5	2	underpressure	500-680
ZA-21	3	underpressure	410-540
ZA-22	5	underpressure	425-580
ZA-26	2.5	underpressure	340-710
ZA-1	1	overpressure	550-630
ZA-6	1	overpressure	320-430
ZA-7	2	overpressure	630-750
ZA-8	1.5	overpressure	350-590
ZA-11	1	overpressure	470-510
ZA-13	1	overpressure	340-600
ZA-16	1	overpressure	250-310 & 420-540
ZA-20	1	overpressure	300-390
ZA-2	2 & 2	overpressure & underpressure	530-570 ; 590-830
ZA-4	2 & 3	overpressure & underpressure	490-560 ; 655-835
ZA-9	1 & 2	overpressure & underpressure	500-560 ; 660-750
ZA-10	2 & 3	overpressure & underpressure	520-570 ; 600-660
ZA-12	2 & 4	overpressure & underpressure	490-560 ; 560-720
ZA-14	1.5 & 2.5	overpressure & underpressure	490-540 ; 590-735
ZA-15	1.5 & 3	overpressure & underpressure	470-520 ; 590-750
ZA-17	1.5 & 2.5	overpressure & underpressure	480-530 ; 620-680
ZA-18	2 & 4	overpressure & underpressure	465-510 ; 560-710
ZA-19	1 & 3	overpressure & underpressure	470-520 ; 720-790
ZA-23	1.5 & 2.5	overpressure & underpressure	540-560 ; 590-710
ZA-24	2 & 2	overpressure & underpressure	550-595 ; 595-720
ZA-25	1 & 2	overpressure & underpressure	490-530 ; 560-730

able in the fracturing report data. However, this data is only available for well ZA-7, with a value of approximately 1106 psi or 7.63 MPa. Consequently, the other wells do not have defined maximum injection limits based on step-rate tests. This pressure represents the threshold at which the formation begins to fracture; therefore, to prevent formation damage or fluid leakage, injection pressures exceeding 1106 psi or 7.63 MPa are not allowed.

4.4. Water Injection Evaluation on Z-600 Layer

This study also includes an injection evaluation in the "ZA" Field, specifically targeting the Z-600 marker. The

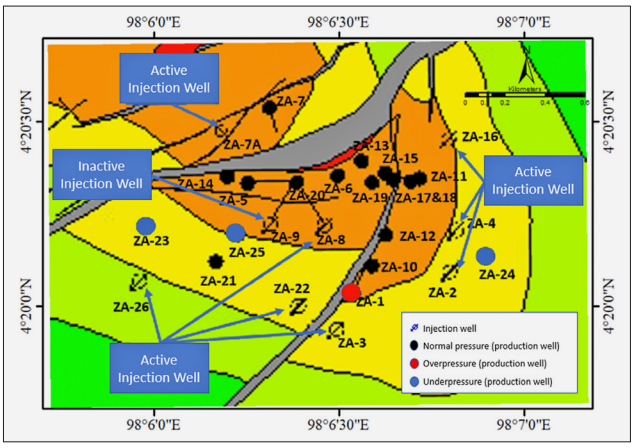

Figure 10. Pore pressure condition after water injection in Z-600 reservoir layer

Z-600 marker refers to a stratigraphic horizon identified from well log responses, and its lateral continuity is limited to log-based correlation across the study wells. It is situated at a depth of approximately 600 meters, with a thickness ranging from 30 to 40 meters. Although the depth varies due to local geological structures, the correlation of this marker does not imply regional geological homogeneity. Wells marked with black circles indicate normal pressure, red circles indicate overpressure, and blue circles indicate underpressure.

Figure 10 shows that, among the production wells, only one well – ZA-1 – experiences overpressure in the Z-600 layer. This overpressure condition is due to the continuous injection of fluid from injection well ZA-3, which causes the pore pressure of ZA-1 to exceed the hydrostatic pressure. This occurs because injection well ZA-3 not only supports production well ZA-1, but also injects fluid into wells ZA-10 and ZA-12 until their pressures return to normal.

Figure 10 also shows production wells that experience underpressure in the Z-600 layer, including wells ZA-24, ZA-23, and ZA-25. Well ZA-23 experiences underpressure despite its proximity to injection wells ZA-2 and ZA-4, which is attributed to its low permeability. The low permeability hinders the flow of injected fluid into the production well. Meanwhile, wells ZA-23 and ZA-25, despite having relatively high permeability, also experience underpressure. This is due to the distance between injection well ZA-22 and production well ZA-23, as well as the fact that injection well ZA-26 is located in a different structural contour than ZA-23. Additionally, well ZA-25 receives injection only from ZA-8, as an injection well ZA-9 has not yet been put into operation. It is assumed that injection well ZA-8 prioritizes injection into production wells within the same structural contour.

Based on this evaluation, it is concluded that the production wells in the "ZA" Field contribute to enhanced oil recovery, although three production wells are still experiencing under-pressure.

5. Conclusions

This study developed a one-dimensional Mechanical Earth Model (1D MEM) that includes elastic properties (Young's modulus and Poisson's ratio), rock strength parameters (UCS, tensile strength, and friction angle), overburden pressure, pore pressure, and minimum horizontal stress. Based on the 1D MEM for each well in the "ZA" Field, several pore pressure anomalies were identified, including over-pressure, under-pressure, and combined overpressure-under-pressure conditions. Underpressure is primarily attributed to fluid depletion from previous production activities, while overpressure results from loading mechanisms.

Each well in the field exhibits UCS values is 42 MPa, tensile strength is 4 MPa, and friction angles ranging from 20° to 31°. These values suggest that the rocks in this field are mechanically weak, likely due to their fine-grained texture. The wells are characterized by shaly sand lithology, which is associated with relatively low friction angles. This is likely due to the unconsolidated nature of the formation, making the rock grains more susceptible to shear under friction. This observation is further supported by reports of sand production events in the "ZA" Field. Additionally, the injection pressure window in each well is relatively wide, both in terms of overpressure (1–2 MPa) and underpressure (1.5–5 MPa). The maximum injection pressure value is currently available only for well ZA-7, recorded at approximately 1106 psi or 7.63 MPa. Therefore, step-rate tests are still required for the remaining wells to determine their actual maximum injection limits.

The results of the geomechanical analysis, particularly through the development of a Mechanical Earth Model (MEM), provide a strong technical basis for defining the safe upper limit of injection pressure. This information directly supports operational decision-making, including injection rate optimization, formation damage risk mitigation, and well planning – ultimately enhancing both safety and field operation efficiency.

Acknowledgement

The authors gratefully acknowledge Pertamina Hulu Rokan for providing the data essential to this research. Sincere appreciation is also extended to any reviewer for their invaluable guidance and supervision throughout the preparation of this manuscript.

6. References

Amin, T., Baroek, M., Santana, S., Sapiie, B. & Gunawan I. (2022). 1D Geomechanical Modeling and Critically-Stressed Fractures Analysis In Naturally Fractured Reservoir, Muara Laboh Geothermal Field, West Sumatra, Indonesia. *Bulletin Of Geology*, *6(1),* 851-865. https://buletingeologi.com/index.php/buletin-geologi/issue/view/15

Astawa, I., Silalahi, I., & Rahardiawan, R. (2012). Geologi Bawah Permukaan Laut Perairan Lembar Peta 0421, Daerah Istimewa Aceh. *Jurnal Geologi Kelautan*, 10(2), 101-115. https://media.neliti.com/media/publications/230393-geologi-bawah-permukaan-dasar-lautperair-f3fb3ce1.pdf.

Attewell P. B. & Farmer I.. W. (1976). Principles of engineering geology. Chapman and Hall, London.

Aziz, A. & Bolt, L.H. (1984). Occurrence and detection of abnormal pressures from geological and drilling data, North Sumatra Basin. *Proc. Indon. Petrol. Assoc*., 13, 194-220.

Birchall, T., Senger, K., & Swarbrick, R. (2022). Naturally Ocuuring Underpressure – A Global Review. *Petroleum Geoscience*, 28. https://doi.org/10.1144/petgeo2021-051?ref=pdf&rel=cite-as&jav=VoR.

Buntoro, A., Rahmad, B., Asmorowati, D., Lukmana, A., Fattah, A. & Anuraga, E. (2022). Overpressure mechanism prediction based on well log and mineralogy analysis from drill cuttings of well NSE-001 in the North Sumatra Basin area, Indonesia. *Journal of Petroleum Exploration and Production Technolog,*. 12, 2801-2815. https://doi.org/10.1007/s13202-022-01482-5.

Collins, P. (2002). Injection Pressures for Geomechanical Enhancement of Recovery Processes in The Athabasca Oil Sands. SPE/Petroleum Society of CIM/CHOA 79028. http://dx.doi.org/10.2118/79028-MS.

Christaras, B., Auger, F., & Mosse, E. (1994). Determination of the moduli of elasticity of rocks. Comparison of the ultrasonic velocity and mechanical resonance frequency methods with direct static methods. *Materials and Structures, 27(4), 222-228*.

Gunawan, A., Sapiie, B., & Wibowo, B. (2017). Analisis Geomekanika Pada Batuan Dasar, Di Area Js-1 Ridge Bagian Selatan, Cekungan Jawa Timur Utara. *Bulletin of Geology*, 1 (1), 1-18. http://dx.doi.org/10.5614/bull.geol.2017.1.1.1.

Knoll, L. (2016). The Process of Building a Mechanical Earth Model Using Well Data.Thesis. Department Petroleum Engineering. Montan University.

Lanin, E. (2021). Rock Mechanical Properties of Indonesian Organic-Rich Shales and Geomechanical Analysis of A Shale Resource Pilot Hole In North Sumatra Basin. Disertasi. Filosofi. University of Wisconsin-Madison.

Larsen, I., Fjaer, E., & Renlie, L. (2000). Static and Dynamic Poisson's ratio of Weak Sandstones. *ARMA North America Rock Mechanics Symposium*.

Linh, D., LOc, N., Tan, V., Huy, N., Trang, N., Tai, P., Abdurrahman, M. & Hidayat, F. (2021). Statistical Estimation of Frictional Coefficients of Faults Based on a Structural Dataset in The Tuy Hoa-Vung Tau Region, Viet Nam. Oil & Gas Science and Technology – Rev. *IFP Energies nouvelles*, 76(35), 1-15. https://doi.org/10.2516/ogst/2021016.

Liu, Y., Liu, S., Zhang, J., and Cao, J. (2025). Real-time estimation of geomechanical characteristics using drilling parameter data and LWD. *Geoenergy Science and Engineering, 244*. https://doi.org/10.1016/j.geoen.2024.213450

Lockner, D. (1995). Rock Failure. *American Geophysical Union*.https://www.researchgate.net/publication/313426883_Rock_failure.

Muchlis & Elder, C. (2020). Structural Style of The North Sumatra Basin, Offshore Aceh. *The 9th AIC 2019 on Sciences*

& Engineering (9thAIC-SE). http://dx.doi.org/10.1088/1757-899X/796/1/012038.

Nuraini, T. (2023). Ketahui Sejarah Lumpur Lapindo Sidoarjo Beserta Penyebab & Dampaknya Bagi Sekitar. https://www.merdeka.com/trending/ketahui-sejarah-lumpur-lapindo-sidoarjo-beserta-penyebab-dampaknya-bagi-sekitar-23578-mvk.html?page=4.

Osborne, M. & Swarbick, R. (1997). Mechanisms for Generating Overpressure in Sedimentary Basins: A Reevaluation. *AAPG Bulletin, V*, 81(6), 1023-1041. https://doi.org/10.1306/522B49C9-1727-11D7-8645000102C1865D.

Perras, M. & Diederichs, M. (2014). A Review of the Tensile strength of Rock: Concepts and Testing. *Geotechnical and Geological Engineering*, 32, 525-546. http://dx.doi.org/10.1007/s10706-014-9732-0.

Prasetyo, A. & Juventa. (2021). Karakterisasi Reservoir Berdasarkan Analisa Avo (Amplitude Versus Offset) Dan LMR (Lambda-Mu-Rho) Di Lapangan "Ap7" Formasi Keutapang Cekungan Sumatra Utara. *Jurnal Teknik Kebumian*, 6(2), 48-60. https://doi.org/10.22437/jtk.v6i02.21184.

Rozamuri, M., Ramdhan, A., & Setiawan, P. (2022). Geologi dan Analisis Geomekanika Terhadap Optimasi Injeksi Air Pada Lapangan "Sarina" Cekungan Sumatra Tengah, Indonesia. *Bulletin of Geology*, 6(3), 1040-1051. https://doi.org/10.5614/bull.geol.2022.6.3.2

Saadatnia, N., Sharghi, Y., Moghadasi, J., & Ezati, M. (2023). Coupled Hydro-mechanical Simulation in The Carbonate Reservoir of A Giant Oil Field in Southwest Iran. *Journal of Petroleum Exploration and Production Technology, 14, 59-83*. https://doi.org/10.1007/s13202-023-01695-2

Shaker, S. (2007). Calibration of Geopressure Predictions Using The Normal Compaction Trend: Perception and Pitfall. http://geopressureanalysis.com/nct_recorded.pdf_final_2pages.pdf.

Shen, S., Gao, Y., & Jia, L. (2024). A comparison of the Relationship between Dynamic and Static Rock Mechanical Parameters. *Applied Sciences, 14*. http://dx.doi.org/10.3390/app14114487

Soepardji, R.. (1983). Geology of The Arun Gas Field. *Society of Petroleum Engineers of AIME*. https://doi.org/10.2118/10486-PA.

Syarifuddin, I. & Ariyanto, P. (2018). Tectono-stratigraphy of Block A area, North Sumatra Basin: The impact of local tectonics and eustasy to accomodation space of the Tertiary interval. *Proceedings, Indonesian Petroleum Association.* http://dx.doi.org/10.29118/IPA18.586.G.

Tampubolon, R., Ozza, T., Arifin, T., Hidayatillah, A., Prasetio, A., & Furqan, T. (2017). A Review of Regional Geology of the North Sumatra Basin and its Paleogene Petroleum System. *Berita Sedimentologi*, 37(1), 23-29. https://doi.org/10.51835/bsed.2017.37.1.95.

Tandirerung, R. (2023). Analisis Geomekanika Batuan Berdasarkan 1D Mechanical Earth Model Sumur B Lapangan X Cekungan Tarakan Provinsi Kalimantan Utara. Skripsi. Program Studi Teknik Geologi. Universitas Hasanuddin. Makassar.

Verma, A., Deb, D., Dey, A., Roy, S., Singh, A., Avadhani, V. & Tiwari, R. (2021). Development of One Dimensional Geomechanical Model for a Tight Gas Reservoir. *Scientific Reports*. https://doi.org/10.1038/s41598-021-00860-z

Wardhana, B., Arsyi, H., Azransyah, T., Mawardi, F., Hafizh, I., & Mulyawan, M. (2021). Fractured Reservoir in Baong Formation, North Sumatra Basin, Indonesia. *Joint Convention Bandung 2021*. Journal.iatmi.or.id.

Wicaksono, A. (2021). Analisis Teknaan Luap dan Hubungannya Terhadap Akumulasi Hidrokarbon di Blok Nunukan, Subcekungan Tarakan. Tesis. Program Studi Teknik Geologi. Institut Teknologi Bandung. Bandung.

Wilson, M., Ansah, S., Nani, S., & Asante, D. (2022). Petrographic Studies And Physico-Mechanical Properties Of Birimian Granitoids – A Case Study Of Oyoko Granitoids Complex In Koforidua. *Geological Behavior*, 6(1), 16-21. http://dx.doi.org/10.26480/gbr.01.2022.16.21.

Yosandian, H. H., Irawan, H., Ulum, B. W. A., Tribuana, I. Y., & Embara, P. (2014). Overpressure Characteristic in the Langkat Field, North Sumatra Basin, Indonesia. *3rd International Conference in Geological and Environmental Sciences*, 73, 40-44.

Zain, M. & Henk, A. (2020). Building 1D and 3D Mechanical Earth Models for Underground Gas Storage – A Case Study from the Molasse Basin, Southern Germany. *Energies*, 13(21), 5722. http://dx.doi.org/10.3390/en13215722.

Zhang, J. (2013). Effective stress, porosity, velocity and abnormal pore pressure prediction accounting for compaction disequilibrium and unloading. *Marine and Petroleum Geology 45*, 2-11. https://doi.org/10.1016/j.marpetgeo.2013.04.007

SAŽETAK

Geomehanička analiza za određivanje maksimalne granice injekcije vode u formaciji Keutapangan, nalazište „ZA", bazen Sjeverna Sumatra

Polje „ZA" nalazi se u bazenu Sjeverne Sumatre i pretežno je pogođeno problemima geotlaka. Zbog toga je geomehanička analiza ključna tijekom bušenja kako bi se ublažile moguće opasnosti. Geomehanička analiza provedena u ovome istraživanju koristi se jednodimenzionalnim mehaničkim modelom Zemlje (1D MEM), koji uključuje sljedeće komponente: naprezanje nadtereta, porni tlak, čvrstoću stijene, elastična svojstva stijena i minimalno horizontalno naprezanje. Podatci korišteni u ovoj analizi prikupljeni su iz sljedećih izvora: mjerenja pomoću žične sonde za sve geomehaničke izračune, testovi tlaka za provjeru vrijednosti pornih tlakova, podatci o gradijentu loma za potvrdu krivulje minimalnoga horizontalnog naprezanja, testovi stupnjevitoga protoka za određivanje granice tlaka injekcije te izvješća s bušotina. Polje „ZA" pokazuje složen režim geotlaka, koji varira od podtlaka do nadtlaka, s prijelaznim zonama koje kombiniraju oba stanja. Nadtlak se uglavnom pripisuje mehanizmima opterećenja, dok je podtlak rezultat povijesne ekstrakcije fluida tijekom prethodnih bušenja. Litološka analiza pokazuje da se rezervoar sastoji od glinovitoga pijeska i sitnozrnatih formacija. Zbog male dubine zakopavanja, ove stijene ostaju slabo konsolidirane, što rezultira uskim sigurnim injekcijskim prozorom iznad pornoga tlaka. Ovo ograničenje prikazano je na primjeru jedne bušotine, gdje je maksimalni dopušteni tlak injekcije iznosio 7,63 MPa, s razmakom od samo 2 MPa iznad pornoga tlaka.

Ključne riječi:
1D MEM, porni tlak, čvrstoća stijena, elastična svojstva stijena, minimalni horizontalni napon

Author's contribution

Zahra Adinda Billqish (B.Sc, Physics, expertise in geophysics, geomechanical analysis) performed the data processing, data analysis, interpretation of the results, and wrote the original draft and edited. **Andika Wicaksono** (M.T., Geology, seismic exploration, petroleum geology) provided the data, data collection, interpretation and supervision. **Sismanto** (Dr in Geophysics, expertise in seismic exploration and rock physics) performed the interpretation and supervision. All authors have read and agreed to the published version of the manuscript.